Martin Wittmaack[1,*]
Markus André[1]
Katharina Schmitz[2]

Dynamic Friction Model for the Investigation of Stick-Slip Oscillations

The optimization of lubricated sealing systems with respect to the stick-slip effect requires a friction model that describes the complex friction behavior in the lubricated contact area. This paper presents an efficient dynamic friction model based on the Stribeck curve, which allows to investigate the influencing parameters through finite element (FE) simulations. The simulation of a tribometer test using this friction model proofs that the model correlates well with the tribometer test results. It is shown that the system stiffness has a significant influence on the stick-slip tendency of the system.

Supporting Information available online

Keywords: Friction-induced oscillation, Friction model, Stick-slip, Stribeck curve

Received: August 30, 2022; *revised:* September 05, 2022; *accepted:* September 09, 2022

DOI: 10.1002/ceat.202200416

1 Introduction

Dynamic seals play an important role in hydraulic systems. Such lubricated parts usually show a quite complex frictional behavior. In this work, special attention is paid to the stick-slip effect, a friction instability in which the contact alternates between sticking and sliding in a frequency range of a few to several thousand hertz. Such friction-induced oscillations result in disturbing squealing noise or positioning inaccuracies of hydraulic parts. Particularly, the frictional behavior in the mixed lubrication regime influences the stick-slip effect [1]. Thus, modeling approaches for an accurate description of the dynamic frictional behavior are required in order to optimize lubricated sealing systems concerning the stick-slip effect.

In previous studies [2], a dynamic friction model based on the Stribeck curve was presented, which describes the buildup and degradation of the lubricating fluid film on a phenomenological basis. In the present paper, the influence of the empirical parameters on the buildup and degradation of the lubricant film is investigated. Furthermore, an approach for the determination of model parameters on basis of the inverse hydrodynamic lubrication method is introduced. The presented friction model is then validated using a tribometer test, which rates the stick-slip tendency of automotive brake fluids. In addition, the influence of the system stiffness on the stick-slip effect is investigated, whereby the system stiffness is varied first by an additional spring [2] and second by modifying the viscoelastic material behavior.

2 Friction Model

2.1 Friction Model in Mixed Lubrication Range

Various approaches exist for modeling the frictional behavior in the mixed lubrication regime, e.g., through description of the friction coefficient by the Stribeck curve or through the calculation of the lubricating fluid film based on the elasto-hydrodynamic lubrication theory (EHL).

The EHL couples the structural mechanics with the fluid mechanics, iterating the solid contact pressure and the pressure in the lubricant film. It is common to use the transient Reynolds equation [3] to describe the lubricant film. Assuming an incompressible Newtonian fluid (density $\rho^{1)}$ = const., viscosity η = const.), this equation depends on the lubricant film height h, the pressure gradient $\partial p/\partial x$, the axial velocities u and the velocities w in radial direction of the moving surfaces a and b:

$$\frac{\partial}{\partial x}\left(\frac{h^3}{12\eta}\frac{\partial p}{\partial x}\right) = \frac{\partial}{\partial x}\left(\frac{u_b + u_a}{2}h\right) + w_a - w_b - u_a\frac{\partial h}{\partial x} \tag{1}$$

Various approaches exist for solving such elasto-hydrodynamic problems [4–6]. However, because of the high computational effort these methods could not be applied successfully to the dynamic stick-slip effect so far.

Another, but simpler approach to designate mixed lubrication is the Stribeck curve, which describes the coefficient of friction as a function of relative velocity based on empirical approaches [7].

The Stribeck curve is indeed commonly used for investigating stick-slip effects. However, this approach describes the

[1]Martin Wittmaack, Prof. Dr.-Ing. Markus André
Martin.Wittmaack@hs-hannover.de
Hochschule Hannover, University of Applied Sciences and Arts, Faculty II – Mechanical and Bioprocess Engineering Department, Ricklinger Stadtweg 120, 30459 Hannover, Germany.

[2]Prof. Dr.-Ing. Katharina Schmitz
RWTH Aachen University, Institute for Fluid Power Drives and Systems (ifas), Campus-Boulevard 30, 52074 Aachen, Germany.

1) List of symbols at the end of the paper.

friction behavior in the stationary state only. Since the fluid volume must enter or leave the lubrication gap during buildup or decrease of the lubricant film, there is a discrepancy between the stationary Stribeck curve and the highly dynamic stick-slip effect. Thus, a suitable simulation approach requires an efficient friction model taking into account the dynamic buildup and degradation of the lubricant film.

2.2 Dynamic Friction Model

As mentioned above, the transient Reynolds equation describes the dynamic of the flow in the lubrication gap. By differentiation and assuming $v_{rel} = u_a - u_b$ and $\partial h/\partial t = w_a - w_b$, the Reynolds equation (1) results in:

$$\frac{\partial h}{\partial t} = \frac{1}{12\eta}\frac{\partial^2 p}{\partial^2 x}h^3 + \frac{1}{4\eta}\frac{\partial h}{\partial x}\frac{\partial p}{\partial x}h^2 - \frac{1}{2}\frac{\partial h}{\partial x}v_{rel} \tag{2}$$

Eq. (2) shows that the time derivative of the lubricating film depends on the second and third power of the lubricating film height h and the relative velocity v_{rel}. In order to avoid the high computational effort of coupling the fluid and structural mechanics, an empirical evolution equation [2] is proposed, describing the evolution of the lubrication gap h:

$$\frac{\partial h}{\partial t} = -\beta\, h^2 + \gamma|v_{rel}| \tag{3}$$

In this empirical equation, the lubricant film is assumed to build up with increasing relative velocity v_{rel}, weighted by the empirical parameter γ and to degrade with the square of the lubricant film height h^2, weighted by the empirical parameter β. For simplification, the term h^3 is neglected. This allows to describe the lubricant film height in stationary state as a function of the relative velocity and to fit the empirical parameters to the solution of the inverse hydrodynamic lubrication method (see Sect. 3.2).

Fig. 1 shows an example for the lubricant film height h during some sudden changes of the relative velocity v_{rel}. The parameters of the investigated fluid RF31 are listed in Tab. 1. With a sudden change in the relative velocity, the lubricant film builds up and degrades with a time delay, whereby the lubricant film height finally converges to the steady-state value.

In the steady state, the lubricant film height depends on the ratio of the empirical parameters γ/β and the relative velocity according to:

$$h_{stat} = \sqrt{\frac{\gamma}{\beta}|v_{rel}|} \tag{4}$$

The duration until the stationary state is reached depends on the empirical parameters γ and β. Fig. 1 also demonstrates the influence of the parameter γ for a constant ratio γ/β. The larger γ is, the faster the fluid film reaches the stationary state.

For the frictional shear stress τ, an additive division into the solid friction τ^s and the fluid friction τ^{fl} is applied according to [2]:

$$\tau = \tau^s + \tau^{fl} \tag{5}$$

An exponential approach [7] is used to describe the solid friction component τ^s. In the stationary state, this approach depends on the contact pressure p, the static friction coefficient μ_0, the relative velocity v_{rel}, and the two empirical Stribeck parameters v_s and δ according to:

$$\tau^s_{stat} = p\,\mu_0\,\exp\left(-\left|\frac{v_{rel}}{v_s}\right|^{\delta}\right) \tag{6}$$

The computation of the transient friction condition requires the determination of the lubricant film height h, which is obtained by integrating Eq. (3) with an explicit Euler scheme. Subsequently, Eq. (4) provides the equivalent relative velocity corresponding to the lubricant film height in the stationary state. Inserting Eq. (4) in Eq. (6) results in the transient solid friction τ^s_{dyn}:

$$\tau^s_{dyn} = p\,\mu_0\,\exp\left(-\left|\frac{\beta\, h^2}{\gamma v_s}\right|^{\delta}\right) \tag{7}$$

Assuming a Couette flow in the lubrication gap, the fluid friction is proportional to the viscosity η, the relative velocity v_{rel}, and the empricial Stribeck curve parameter c and inversely proportional to lubricant film height h according to:

$$\tau^{fl} = c\,\eta\frac{v_{rel}}{h} \tag{8}$$

From Eqs. (4) and (8), the fluid friction in a stationary state can be expressed as a function of the relative velocity v_{rel}. This allows the Stribeck curve parameter c to be determined from measured Stribeck curves.

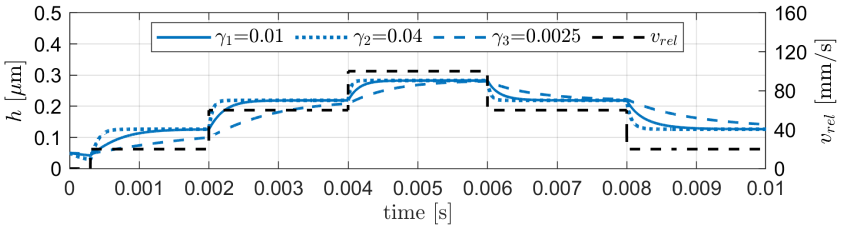

Figure 1. Buildup and degradation of the lubricant film.

3 Validation of the Dynamic Friction Model

A validation of this dynamic friction model is carried out with an SRV®-tribometer test with which the stick-slip tendency of brake fluids is characterized. This test is performed and simulated with two fluids, which show significant differences in the stick-slip behavior.

3.1 Characterization of the Investigated Fluid

In order to validate the dynamic friction model, the automotive brake fluids RF31 and RF33 are characterized. In tribometer tests as well as in product tests, the use of fluid RF31 results in a strong stick-slip behavior in the sealing system of the master brake cylinder, while the use of fluid RF33 does not.

The viscosity of these two fluids was measured using a viscometer with a coaxial cylinder measuring system by the Deutsche Institut für Kautschuktechnologie e.V. (DIK e.V.) [9]. At a temperature of $T = 23\,°C$, the viscosity differs only slightly ($\eta_{RF31} = 11.5$ mPa s, $\eta_{RF33} = 12.2$ mPa s).

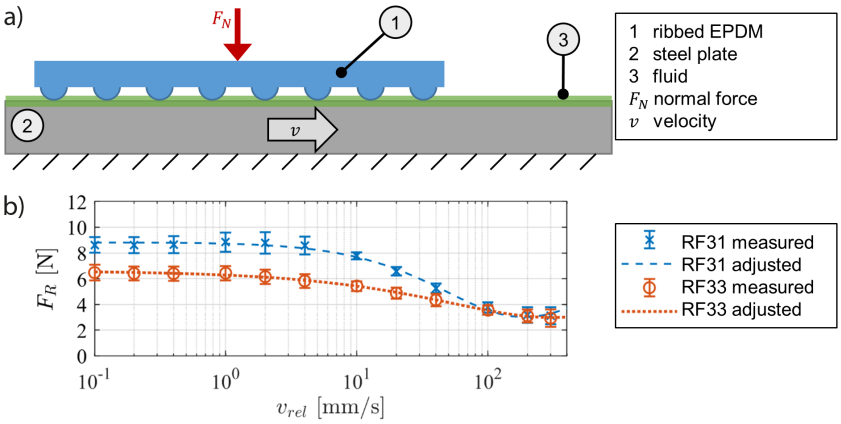

Figure 2. Linear tribometer test (a) to measure the Stribeck curves, (b) of the investigated fluids [2].

For characterization of the friction properties, the Stribeck curves of the two fluids were measured with a linear tribometer also by the DIK e. V. [9]. In this test, a rubber plate with rib structure is moved on a C45 steel plate (Fig. 2a), which is ground transverse to the direction of movement. The rubber plate (length 32 mm, width 20 mm, thickness 2 mm) has eight semi-circular ribs (radius r = 1 mm) and is made of ethylene propylene diene monomer (EPDM) with hardness 80 ShA [9].

Fig. 2b presents the measured Stribeck curves of the fluids RF31 and RF33 with a normal force $F_N = 29.98$ N in the velocity range $v_{rel} = 0.1, \ldots, 300$ mm s^{-1}. Both fluids differ particularly in the range of boundary friction. Thus, at a relative velocity of $v_{rel} = 0.1$ mm s^{-1}, the coefficient of friction of fluid RF31 is $\mu_{RF31} = 0.2877$ ($F_{R\ RF31} = 8.6$ N), whereas for the fluid RF33 it is $\mu_{RF33} = 0.2159$ ($F_{R\ RF33} = 6.5$ N). In the mixed lubrication regime, the coefficient of friction of fluid RF31 drops faster than that of the fluid RF33. At a relative velocity of $v_{rel} = 100$ mm s^{-1}, the friction forces of both fluids are almost identical. Also the result of the friction approach according to Eqs. (4), (5), (6) and (8) is visualized with parameters fitted to the measured data.

3.2 Determination of the Dynamic Friction Model Parameters

The ratio of the empirical parameters γ/β is determined using the inverse hydrodynamic lubrication (IHL) method according to Blok [10]. More recent examples for the implementation of the IHL method are given in [11] and [12]. This method computes the profile of the lubricant film height under a single rib of the linear tribometer test (Fig. 2a) for a given relative velocity in the stationary state. The required contact pressure distribution is computed with a static finite element (FE) simulation using the material model described in Sect. 3.5. The ratio of the empirical parameters γ/β is adjusted at the position of the minimum lubricant film height, since friction has a maximum at this position.

Fig. 3 displays the minimum lubricant film height from the IHL method as a function of relative velocity in good accordance with the dynamic friction model. The investigation of the empirical parameter γ in Fig. 1 shows that the stationary solution is obtained faster with increasing parameter γ. The empirical parameter γ is then manually adjusted to the test data from the SRV®-tribometer test (Sect. 3.3).

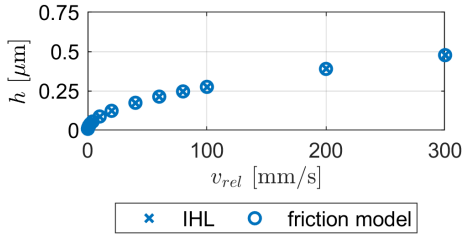

Figure 3. Computation of the lubricant film height under the rib of the linear tribometer test.

By minimizing the error norm, the Stribeck parameters μ_0, v_s, δ, and c are adjusted to the measured Stribeck curves (Fig. 2b). Here, the friction force $F_R = \tau A$ in stationary state is determined from Eqs. (4), (5), (6) and (8) according to:

$$F_R = F_N\,\mu_0\,\exp\left(-\left|\frac{v_{rel}}{v_s}\right|^{\delta}\right) + A\,c\,\eta\left(\frac{\beta}{\gamma}|v_{rel}|\right)^{\frac{1}{2}} \tag{9}$$

The normal force F_N during the tribometer test is known and the contact area A is estimated with an FE model of the test setup. Fig. 2b demonstrates that Eq. (9) fits well to the measured Stribeck curves. Tab. 1 lists the corresponding Stribeck parameters. Particularly, the solid friction parameters μ_0, v_s, and δ of the two investigated fluids RF31 and RF33 differ.

3.3 SRV®-Tribometer Test

A study on the stick-slip tendency of brake fluids shows that the SRV®-tribometer (Fig. 4) of the company Optimol well

Table 1. Parameters of the Stribeck curve.

Fluid	μ_0 [–]	v_s [mm s^{-1}]	δ [–]	c [–]	β [mm^{-1}s^{-1}]	γ [–]	F_N [N]	A [mm^2]
RF31	0.2928	57.28	0.8859	7.86	12.51×10^6	0.01	29.98	57.2
RF33	0.2204	94.15	0.5832	4.81	12.41×10^6	0.01	29.98	57.2

reproduces observations from product tests [13, 14]. In this test, the tribometer presses a steel ball with a diameter of 10 mm (Item 1) onto an EPDM rubber specimen (Item 3) with a defined normal force F_N = 15, …, 25 N. The cylindrical rubber specimen has a thickness of t = 2 mm and a diameter of 10 mm. It is fixed within a steel trough (Item 4) and is fully covered by the fluid (Item 2) to be tested.

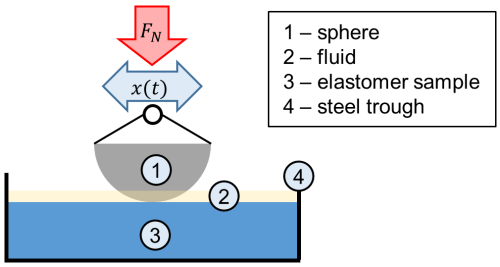

Figure 4. SRV®-tribometer test.

The steel ball (sphere) performs an oscillating motion $x(t)$ with the frequency f_a = 2, …, 6 Hz and an amplitude a = 1 mm according to:

$$x(t) = a \sin(2\pi f_a\, t) \tag{10}$$

In order to achieve reproducible test results, the vulcanization skin needs to be removed before the test. A possibility is to grind off the vulcanization skin with sandpaper (400 grit). In this case, the sandpaper was pressed on the rubber specimen with a normal force of F_N = 50 N while moved with the frequency f_a = 1 Hz and an amplitude a = 50 mm for 20 s according to Eq. (10).

Fig. 5 shows the ratio of the friction force to the normal force F_R/F_N for the SRV®-tribometer test depending on the movement of the sphere $x(t)$ at the frequency of excitation f_a = 5 Hz, an amplitude a = 1 mm, and a normal force F_N = 20 N. The experiments were carried out at the Kompetenzzentrum Tribologie of the Hochschule Mannheim [14]. It is obvious that the stick-slip effect occurs with Fluid RF31 (blue line), but not with Fluid RF33 (orange line).

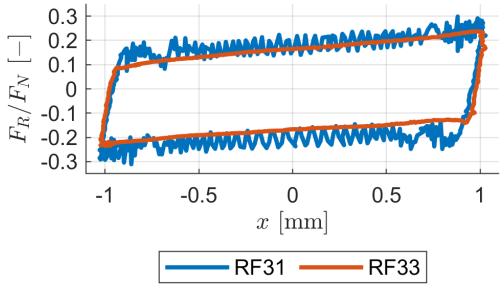

Figure 5. Measured ratio of friction force to normal force of the SRV®-tribometer test with two fluids [2].

3.4 FE Simulation

During a stick-slip situation, the contact changes between sticking and sliding at a high frequency. This friction-induced oscillation results in a corresponding fast change of velocities and accelerations. For numerical reasons, an explicit time integration scheme is used for the dynamic FE simulation of the stick-slip effect. In the present work, the commercial simulation software ABAQUS/explicit is used for this purpose [8].

In the FE simulation model of the SRV®-tribometer (Fig. 4), the sphere (Item 1) as well as the steel trough (Item 4) are assumed to be rigid surfaces, since their deformation is negligible compared to the elastomer plate. The rubber specimen (Item 3) is meshed with linear hexahedral elements (element type C3D8R). To reduce the computation time, the symmetry of the experimental setup is considered and only half of the model is used. In the contact between the sphere (Item 1) and the rubber sample (Item 3) the dynamic friction model is applied, while the contact between the rubber sample (Item 3) and the steel trough (Item 4) a Coulomb friction law with friction coefficient of μ = 0.3 is assumed.

The simulation consists of three steps. In the first simulation step, the steel ball is pressed onto the rubber sample with a specified force. Due to the viscoelastic material behavior of the rubber, a simulation step follows in which the dynamic effects decay. In the third simulation step, the response of the SRV®-tribometer test is computed, whereby the steel ball is periodically moved with a displacement $x(t)$ according to Eq. (10).

3.5 Material Model

The investigated EPDM rubber was characterized by the DIK e.V. [9]. The hyperelastic Neo-Hooke material model is used for the elastic response of the investigated EPDM. The strain energy density W of the compressible Neo-Hooke material model is determined from the Neo-Hooke parameter C_{10}, the first invariant $\hat{I}_1$ of the Cauchy-Green tensor, compressibility parameter D_1, and the elastic volume ratio J^{el}:

$$W = C_{10}\left(\hat{I}_1 - 3\right) + \frac{1}{D_1}\left(J^{el} - 1\right)^2 \tag{11}$$

The elastic response is determined from an uniaxial tension test and yields a Neo-Hooke parameter C_{10} = 1.1612 MPa [2]. Due to the explicit time integration scheme it is necessary to assume a moderate volumetric compressibility with $D_1 = 2/K$ = 0.1 MPa^{-1}, where K denotes the bulk modulus.

The viscoelastic material behavior of the EPDM rubber is described by a generalized Maxwell model in the form of a

Prony series. The shear storage modulus G' and the shear loss modulus G'' [15] depend on the Prony parameters G_i, the relaxation times τ_i^{p} of the individual Prony elements, and the frequency f as follows:

$$G'(f) = G_\infty + \sum_{i=1}^{n} \frac{G_i \left(\tau_i^{\mathrm{p}} 2\pi f\right)^2}{1 + \left(\tau_i^{\mathrm{p}} 2\pi f\right)^2} \tag{12}$$

$$G''^{(\mathrm{f})} = \sum_{i=1}^{n} \frac{G_i \tau_i^{\mathrm{p}} 2\pi f}{1 + \left(\tau_i^{\mathrm{p}} 2\pi f\right)^2} \tag{13}$$

The shear storage modulus additionally depends on the static shear modulus G_∞, which is determined from the Neo-Hooke parameter C_{10} according to:

$$G_\infty = 2C_{10} \tag{14}$$

By minimizing the error norm, the Prony parameters are fitted to a master curve at reference temperature $T_{\mathrm{ref}} = 20\,^{\circ}\mathrm{C}$, which is received from a dynamic mechanical analysis of the EPDM rubber [2]. In order to reduce the required relaxation time in the simulation model, the Prony series is reduced so that the maximum relaxation time is $\tau_{\mathrm{p\ max}} = 0.4\,\mathrm{s}$. Since the minimum SRV® excitation frequency $f_{\mathrm{a}} = 2\,\mathrm{Hz}$ is of the same order of magnitude as the maximum relaxation time and the expected minimum stick-slip frequency is about 500 Hz, the error resulting from this assumption is expected to be negligible.

3.6 Simulation Results

Fig. 6 depicts the ratio of the friction force to the normal force $F_{\mathrm{R}}/F_{\mathrm{N}}$, achieved from a high-resolution finite element simulation using the dynamic friction model compared with the experimental results of the SRV® test. It is obvious that for the fluid RF31 the stick-slip effect occurs in the FE simulation as well as in the tribometer test. In contrast, the stick-slip effect does not occur for fluid RF33. Compared with the test results, the FE simulation computes a larger oscillation amplitude for the fluid RF31. Despite the difference in amplitude, the simulation results correlate very well with the experimental observations.

In contrast to the dynamic friction model, the stationary Stribeck curve does not take into account the buildup and degradation of the lubricant film. If this stationary friction model is used instead, the stick-slip effect occurs with both fluids RF31 and RF33 (Fig. 7). Thus, the use of a stationary Stribeck curve is not sufficient to provide an accurate stick-slip prediction. Consequently, it is important to consider the buildup and degradation of the lubricant film in dynamic friction modeling.

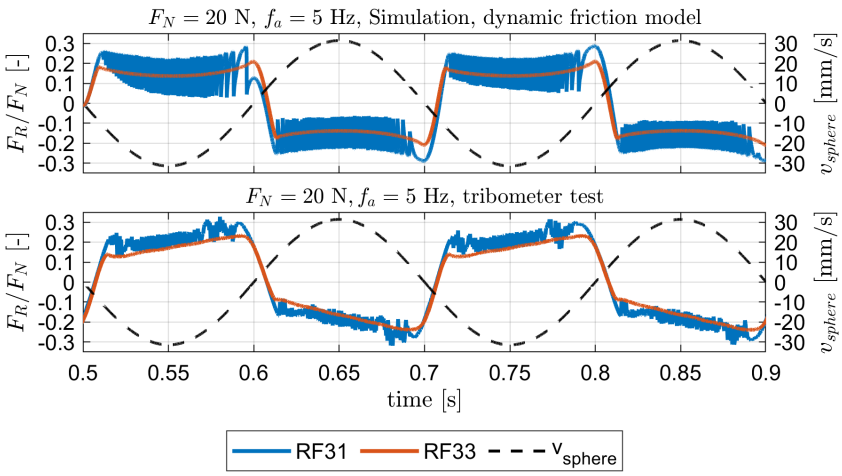

Figure 6. FE simulation of the SRV®-tribometer test with dynamic friction model and test result [2].

4 Influence of Stiffness

Observations from the SRV®-tribometer tests show that the sensitivity of the test strongly depends on the system stiffness of the tribometer. Depending on the selected stiffness of the test setup, the stick-slip effect may or may not be excited. Therefore, in this chapter the influence of stiffness on the stick-slip effect is investigated using the presented FE simulation approach.

4.1 Variation of Stiffness by Additional Spring

The stiffness k of the system [16] is determined during the sticking period by the derivative of the friction force $F_{\mathrm{R}}(t)$ with respect to the displacement $u(t)$ according to:

$$k = \frac{\mathrm{d}F_{\mathrm{R}}}{\mathrm{d}u} \approx \frac{F_{\mathrm{R}}(t + \Delta t) - F_{\mathrm{R}}(t - \Delta t)}{u(t + \Delta t) - u(t - \Delta t)} \tag{15}$$

In the simulations of Sect. 3, only the elasticity of the rubber specimen was taken into account and the rest of the test setup was assumed rigid. In the present section, the system stiffness is artificially reduced by introducing an additional spring into the simulation model. A detailed description of the simulation model with the additional spring can be found in the Supporting Information. Now the stick-slip effect can be excited for a previously unobtrusive system [2, 8].

Fig. 8 shows the friction force F_{R} and the stiffness k depending on the displacement u of the sphere. In the simulation model for fluid RF33 without additional spring, no stick-slip occurs. Here, the initial stiffness of the simulation model is $k \approx 150\,\mathrm{N\,mm^{-1}}$. The integration of an additional spring with a stiffness of $k_{\mathrm{spring}} = 200\,\mathrm{N\,mm^{-1}}$ and a low damping of $d = 0.02\,\mathrm{N\,s\,mm^{-1}}$ reduces the initial system stiffness to $k \approx 80\,\mathrm{N\,mm^{-1}}$ and clearly initiates the stick-slip effect. This proves that the stick-slip tendency increases with decreasing stiffness [2].

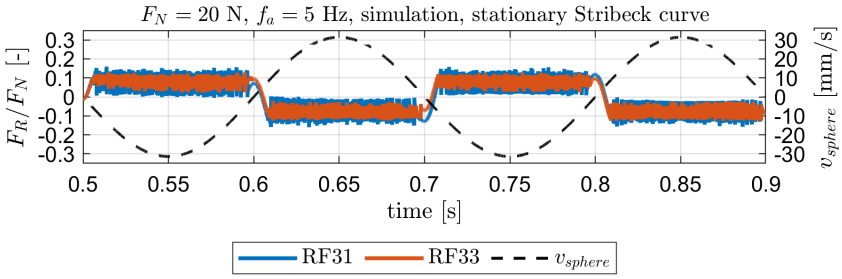

Figure 7. FE simulation of the SRV®-tribometer test with stationary friction model [2].

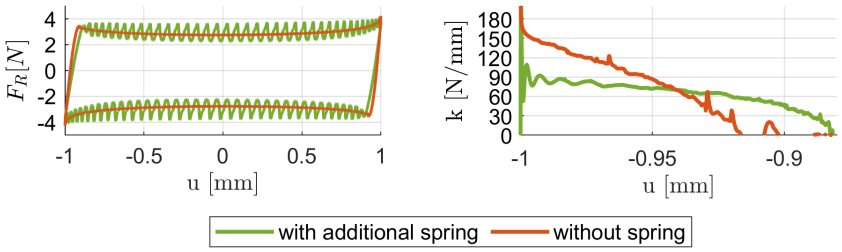

Figure 8. Influence of system stiffness on stick-slip effect with fluid RF33 [2].

4.2 Variation of Stiffness by Changing the Viscoelastic Material Properties

The previous chapter shows that the stiffness of the tribological system influences the stick-slip tendency. The following chapter investigates the influence of material properties on the stick-slip effect. For this purpose, the viscoelastic material behavior is artificially varied by modifying the Prony parameters G_i. Reducing the Prony parameter values G_i by 50 % corresponds to a reduction of elastic and damping properties of the rubber material. On the one hand, this also results in a reduction of the initial stiffness from $k \approx 150\,\mathrm{N\,mm^{-1}}$ to $k \approx 100\,\mathrm{N\,mm^{-1}}$ (Fig. 8), which again provokes a slight stick-slip tendency with the fluid RF33. Compared with Fig. 8, the stick-slip effect in Fig. 9 is less severe because the dynamic mechanisms are different. On the one hand, the modification of the Prony parameters also change the system damping. On the other hand, the additional spring (Fig. 8) yields other oscillation modes than a purely displacement driven sphere.

Fig. 9 indicates that reducing the Prony parameter G_i reduces the system stiffness k in such a way that the stick-slip effect is provoked. Now an increase of the system stiffness is investigated. For this purpose, the friction model of the fluid RF31, in which the stick-slip effect originally occurs, is used. Assuming double values for the Prony parameters G_i leads to an increase of the initial stiffness from $k \approx 150\,\mathrm{N\,mm^{-1}}$ to $k \approx 240\,\mathrm{N\,mm^{-1}}$. From the results in Fig. 10 it is clear that this suppresses the stick-slip effect.

The study demonstrates that by modifying the viscoelastic material behavior the system stiffness can be influenced. In general, a stiffness reduction leads to an increase in the stick-slip tendency, while a stiffness increment reduces it. These experimental results correlate well with basic investigations on the stiffness influence on the stick-slip effect. Examples with a simple spring-mass-damper system are shown in [8]. Consequently, the system stiffness must be carefully selected for an appropriate investigation of stick-slip phenomena.

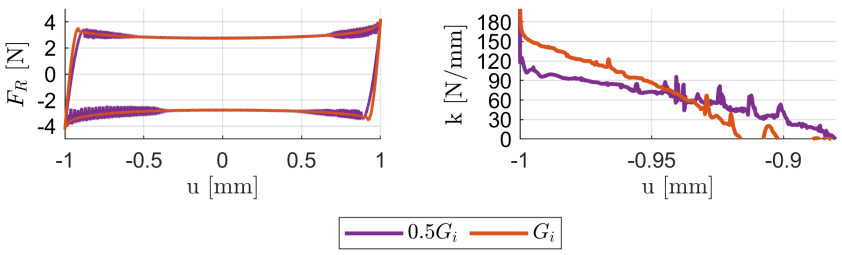

Figure 9. Influence of viscoelastic material properties on stick-slip effect with RF33.

5 Summary and Conclusion

The optimization of lubricated sealing systems with regard to the stick-slip effect requires an efficient dynamic friction model. The common approach of a Stribeck curve describes the frictional behavior in the stationary state only. However, the much more accurate EHL simulation approaches go along with high computational effort and convergence issues. Thus, they are not applied for stick-slip computations in this work. In contrast, the friction model presented in this work describes the dynamics of the lubrication film through a phenomenological extension the stationary Stribeck curve. The computations of SRV®-tribometer tests are performed for two different fluids with different stick-slip tendency. These simulation results correlate very well with the experimental results.

Furthermore, the phenomenological dynamic friction model is used to investigate the influence of stiffness on the stick-slip effect with the introduced simulation model. A reduction of the system stiffness is achieved by adding an additional spring to the test setup and by modifying the viscoelastic material behavior. Both approaches are able to provoke the stick-slip effect for previously inconspicuous systems. In contrast, increasing the system stiffness results in a suppression of the stick-slip effect. This study shows that the system stiffness has a huge influence on the stick-slip effect and its increase reduces the stick-slip tendency of lubricated systems.

The presented dynamic friction model is useful in the development of dynamic hydraulic sealing systems, helping to avoid disturbing stick-slip effects. Although the physical motivation and determination of the empirical parameters β and γ requires further work, the presented approach enables a good qualitative and quantitative representation of stick-slip mechanisms in lubricated friction systems. A starting point

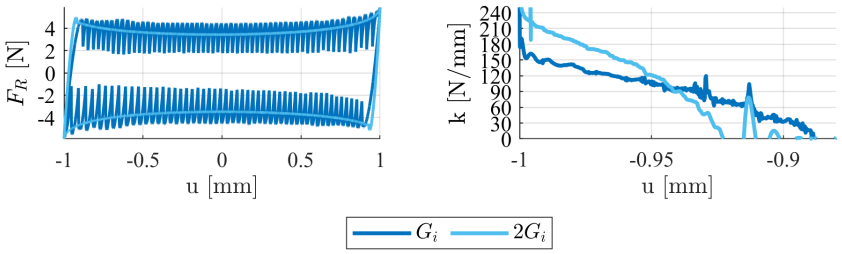

Figure 10. Influence of viscoelastic material properties on stick-slip effect with RF31.

for a more detailed investigation of the lubrication film buildup and degradation could be based on the EHD approaches of [5] and [6].

Supporting Information

Supporting Information for this article can be found under DOI: https://doi.org/10.1002/ceat.202200416.

Acknowledgment

The authors thank the Deutsche Institut für Kautschuktechnologie e.V. (DIK e.V.) for providing the Stribeck curves and for the characterization of the DIK reference elastomer. We also like to thank the Kompetenzzentrum Tribologie of the Hochschule Mannheim (KTM) for providing the SRV®-tribometer test results. Open access funding enabled and organized by Projekt DEAL.

The authors have declared no conflict of interest.

Symbols used

a	[mm]	amplitude
A	[mm^2]	contact area
c	[–]	Stribeck curve parameter
C_{10}	[MPa]	Neo-Hooke parameter
d	[N s mm^{-1}]	damping parameter
D_1	[MPa^{-1}]	compressibility
f	[s^{-1}]	frequency
f_a	[s^{-1}]	frequency of SRV®-tribometer
F_N	[N]	normal force
F_R	[N]	friction force
G	[MPa]	shear modulus
G'	[MPa]	shear storage modulus
G''	[MPa]	shear loss modulus
G_i	[MPa]	Prony parameter
G_∞	[MPa]	static shear modulus
h	[µm]	lubricant film height
$\hat{I}_1$	[–]	first invariant of Cauchy-Green tensor
J^{el}	[–]	elastic volume ration
k	[N mm^{-1}]	stiffness
K	[MPa]	bulk modulus
p	[MPa]	pressure
t	[s]	time
T	[°C]	temperature
u_a, u_b	[mm s^{-1}]	velocity in axial direction
v_{rel}	[mm s^{-1}]	relative velocity
v_s	[mm s^{-1}]	Stribeck curve velocity parameter
w_a, w_b	[mm s^{-1}]	velocity in radial direction
W	[MPa]	strain energy density
x	[mm]	sphere movement

Greek letters

β	[mm^{-1}s^{-1}]	empirical fluid film parameter
γ	[–]	empirical fluid film parameter
δ	[–]	Stribeck curve parameter
η	[mPa s^{-1}]	viscosity
μ	[–]	static friction coefficient
μ_0	[–]	Stribeck curve parameter
ρ	[t mm^{-3}]	density
τ	[MPa]	shear stress
τ_p^i	[s]	relaxation time of Prony element

Abbreviations

EHL	elasto-hydrodynamic lubrication theory
EPDM	ethylene propylene diene monomer
FE	finite element
IHL	inverse hydrodynamic lubrication

References

[1] R. A. Ibrahim, *Appl. Mech. Rev.* **1994**, *47 (7)*, 209–226. DOI: https://doi.org/10.1115/1.3111079
[2] M. Wittmaack, M. André, J. Molter, *Tribol. Schmier.* **2022**, *69 (1)*, 5–14. DOI: https://doi.org/10.24053/TuS-2022-0002
[3] *Fundamentals of Fluid Film Lubrication*, 2nd ed. (Eds: B. J. Hamrock, S. R. Schmid, B. O. Jacobson), Marcel Dekker, New York **2004**.
[4] D. Bartel, *Simulation von Tribosystemen. Grundlagen und Anwendungen*, Vieweg + Teubner, Wiesbaden **2010**.
[5] T. Schmidt, M. André, G. Poll, *Tribol. Int.* **2010**, *43 (10)*, 1775–1785. DOI: https://doi.org/10.1016/j.triboint.2009.11.012
[6] J. Angerhausen et al., *Int. J. Fluid. Power* **2019**, *20 (1)*, 1–26. DOI: https://doi.org/10.13052/ijfp1439-9776.2011
[7] B. Armstrong-Hélouvry, *Control of Machines with Friction*, Springer, Boston, MA **1991**.

[8] M. André, M. Wittmaack, *Schlussbericht zum ögP Tribologie in Normen weltweit (TriNoWe) im Rahmen des BMWi-Förderprogramms WiPaNo*. Hochschule Hannover, **2021**. DOI: https://doi.org/10.2314/KXP:1767529422
[9] A. Lang, *Tribologie in Normen weltweit (TriNoWe): Abschlussbericht: im Rahmen des BMWI-Förderprogramms WiPaNo. Deutsches Institut für Kautschuktechnologie*, **2021**. DOI: https://doi.org/10.2314/KXP:1767532911
[10] H. Blok, in *Int. Symp. On Lubrication and Wear* (Eds: D. Muster, B. Sternlicht), McCutchan, Berkeley, CA **1965**.
[11] A. F. C. Kanters, J. F. M. Verest, M. Visscher, *Tribol. Trans.* **1990**, *33 (3)*, 301–306. DOI: https://doi.org/10.1080/10402009008981959
[12] A. Fatu, M. Hajjam, *Proc. Inst. Mech. Eng. J.: J. Eng. Tribol.* **2011**, *225 (12)*, 1159–1173. DOI: https://doi.org/10.1177/1350650111417046
[13] M. Hilden, in *Reibung, Schmierung und Verschleiß: 62. Tribologie-Fachtagung 2021*, Gesellschaft für Tribologie, Aachen **2021**, 329–341.
[14] J. Molter, *Schlussbericht zum ögP Tribologie in Normen weltweit (TriNoWe) im Rahmen des BMWi-Förderprogramms WiPaNo*. Hochschule Mannheim, **2021**. DOI: https://doi.org/10.2314/KXP:1811661947
[15] *FEM zur Berechnung von Kunststoff- und Elastomerbauteilen*, 2nd ed. (Eds: M. Stommel, M. Stojek, W. Korte), Hanser, München **2018**.
[16] M. Lindner, Experimentelle und theoretische Untersuchungen zur Gummireibung an Profilklötzen und Dichtungen, *Ph.D. Thesis*, Universität Hannover **2006**.

